ACS APPLIED MATERIALS & INTERFACES

www.acsami.org

Research Article

Laminar Flow-Based Fiber Fabrication and Encoding via Two-Photon Lithography

Xiaobao Cao, Quan Gao, Shangkun Li, Songtao Hu, Jing Wang, Peter Fischer, Stavros Stavrakis,* and Andrew J. deMello*

Cite This: *ACS Appl. Mater. Interfaces* 2020, 12, 54068−54074

Read Online

ACCESS | Metrics & More | Article Recommendations | Supporting Information

ABSTRACT: In recent years, flow photolithography (FL) has emerged as a powerful synthetic tool for the creation of barcoded microparticles with complex morphologies and chemical compositions which have been shown to be useful in a range of multiplexed bioassay applications. More specifically, FL has been highly successful in producing micron-sized, encoded particles of bespoke shape, size, and color. That said, to date, FL has been restricted to generating barcoded microparticles and has lacked the ability to produce hybrid fibers which are structurally and spectrally encoded. To this end, we herein present a method that combines a continuous flow microfluidic system with two-photon polymerization (2PP) to fabricate microscale-encoded fibers and Janus strips in a high-throughput manner. Specifically, two co-flow liquid streams containing a monomer and initiator are introduced through a Y-shape channel to form a stable interface in the center of a microfluidic channel. The flow containing the (fluorescently labeled) monomer is then patterned by scanning the voxel of the 2PP laser across the interface to selectively polymerize different regions of the forming fiber/particle. Such a process allows for rapid spectral encoding at the single fiber level, with the resulting structurally coded fibers having obvious application in the fields of security identification and anticounterfeiting.

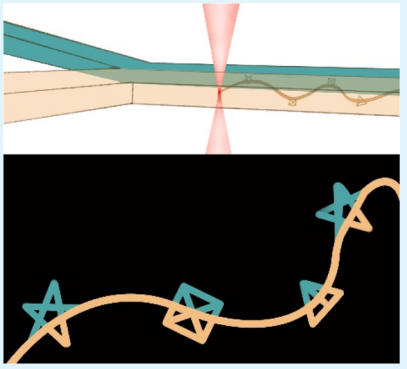

KEYWORDS: *microfluidics, laminar flow, two-photon polymerization, hybrid fiber, barcoding*

1. INTRODUCTION

Barcodes are an integral part of everyday life and have become the most popular data entry method to track the ever-exploding amounts of information. Although barcodes are widely used around the world in many retail, IT, and healthcare settings, they have also found great utility in the identification and tracking of biological entities when performing multiplex assays. Indeed, many contemporary platforms for gene profiling, small-molecule screening, and clinical diagnostics incorporate multiplexed assays.[1] In this context, barcoded microparticles have attracted considerable attention as a tool for assay registration and identification.[2] Encoded nanoparticles and microparticles represent a novel class of detection and identification tool for bioanalysis.[3] Such particles can be synthesized in a number of different ways and can be encoded through variations in shape, composition, morphology, and optical properties.[4−9] For example, microparticles decorated with probe molecules able to react with a given target can be unambiguously identified through their barcode.[2,10] Additionally, encoded microparticles can serve as a solid-phase support for a given product, thus linking the particle code to the identity of the product and its associated history.[11] Accordingly, much interest is currently focused on improving encoding methods, in regard to its speed, encoding capabilities, and robustness, with a view to enable a range of novel multiplexed assay platforms for biological experimentation.[12]

In simple terms, the production of encoded microparticles relies on creating particles with defined shape,[6] size,[13] and color.[12] Many encoding strategies have been developed to generate such barcoded particles at high throughput.[14−17] Existing encoding methods generally fall into one of two categories, namely, spatial encoding or optical encoding.[3,18] Spatial encoding schemes create graphical patterns or barcodes in the particle material in a variety of ways.[8,19] Although useful, spatial methods are compromised by their complexity, cost, inability to generate large encoded populations, and inefficient readout methods. Conversely, optical encoding methods produce spectral features that can be identified in a non-invasive and non-destructive manner, thereby exploiting the advantageous capability of optical multiplexing.[12,20−24] Spectral encoding schemes typically incorporate mixtures of photoluminescent materials such as lanthanides,[25,26] quantum dots

Received: August 18, 2020
Accepted: October 29, 2020
Published: November 10, 2020

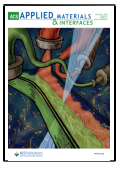

https://dx.doi.org/10.1021/acsami.0c14917
ACS Appl. Mater. Interfaces 2020, 12, 54068−54074

(QDs),[27−31] and fluorescent dyes[32] that emit radiation at different wavelengths and thus generate uniquely identifiable signatures. Such schemes allow identification of codes in any orientation and are compatible with conventional bead synthetic procedures and standard detection systems. Despite the obvious promise of spectral encoding schemes, intrinsic technical challenges have limited their practical application. First, organic fluorophores have broad emission bandwidths, reduced Stokes shifts, and poor photostabilities,[33,34] making it difficult to unambiguously decode emission contributions from multiple fluorophores because of their spectral overlap. QDs provide for narrow and tunable excitation and emission spectra and have therefore been the subject of considerable recent interest for encoding schemes.[28] That said, despite their optical advantages, their high costs significantly limit accessible coding capacities.[35] As a result, the largest experimentally produced spectral code sets from organic dyes or QDs have fallen well short of theoretical expectations.[36] In addition, most spectral encoding applications have been limited to biological multiplexing studies and lack the robustness and reusability features required for industry barcoding, such as in blockchain technology.

In general, the generation of large populations of encoded particles is limited by the technical difficulties associated with producing more than a few hundred unique codes.[37] In simple terms, the number of distinct barcode particles that can be produced by a given method is limited by intrinsic defects in the encoding strategies and the lack of effective synthetic methods that operate on short timescales. In recent years, microfluidic technologies have created new and exciting opportunities to prepare microparticles of variable morphology and composition.[38−42] When combined with continuous-flow microfluidics, high-throughput flow-lithography approaches pioneered by Doyle and colleagues can be used for fabricating encoded microstructures.[19] Although powerful, stop-flow lithography (SFL) is limited in throughput by the need to stop the flow of a liquid prepolymer in the channel prior to each curing step.[43] Improvements in throughput have been realized through the demonstration of continuous-flow lithography (CFL), where lithographic curing occurs as the liquid prepolymer flows.[44−47] However, most flow-lithography approaches produce geometries that are limited in resolution and shape (i.e., only 2D patterns can be extruded) and require the use of an oxygen inhibition layer. Accordingly, new processing technologies are needed for the fabrication and integration of functional 3D microstructures. In this regard, additive manufacturing via two-photon polymerization (2PP) is a promising method to achieve such a goal due to its programmability, 3D processing capabilities, and high spatial resolution.[48,49]

Due to their inherent anisotropy, fibers are potentially useful for barcoding applications. Indeed, microfluidic schemes have been successfully used to produce multicompartment fibers of complex shape and composition.[50] For example, microfluidic spinning approaches provide flexibility and reproducibility in the synthesis of uniform-sized fibers with adjustable composition, a process inspired by the natural process of silk spinning in spiders or silkworms.[51−53] Using such a tactic, fibers with a variety of structures can be produced, including flat fibers,[54] Janus structures,[55] spiral curls,[56] and bamboo-like architectures.[57] To control the chemical composition and morphology of microfibers, a microfluidic device comprising co-axial glass capillaries has been used to synthesize coded alginate microfibers.[58] In addition, Hwang et al. presented a multiphase parallel co-flow PDMS microdevice to fabricate hollow fibers with adjustable compartments and heterogeneous payloads in a single step.[59] Using such an approach, multicompartment microfibers allowed the synthesis of solid poly(lactic-*co*-glycolic acid) fibers for cell culturing purposes. Additionally, Yu et al. employed a multibarrel capillary microdevice with multiple flows to fabricate hollow Janus alginate microfibers.[60] That said, although microfluidic spinning is a powerful approach for the preparation of microfibers with complex structures, there are still challenges associated with the high throughput fabrication of hybrid fibers (containing structural patterns and spatiotemporal variations in color) when cross sections fall below 10 μm.[61] In addition, although two-photon CFL allows the creation of polymeric fibers and with sub diffraction resolution,[49] the fabrication of complex hybrid fiber structures has not yet been demonstrated. To address these limitations, we herein combine 2PP and microfluidic laminar flow processing to fabricate bespoke multicomponent microfibers at throughputs well in excess of any existing method and with a superior resolution than the existing photomask-based flow lithography methods. The key novelty in this approach lies in the ability to rapidly fabricate 2D microfibers in flow, significantly reducing fabrication timescales. By scanning the excitation laser rapidly using a mirror galvanometer, polymerization can be carried out across co-flowing streams to generate Janus microfibers containing user-defined encoding morphologies. Such an encoding method can be used to prepare fibers of different lengths and variable composition, thus allowing the introduction of spatial patterns and unique optical signatures at the single fiber level.

2. RESULTS AND DISCUSSION

Conventional photoinduced polymerization methods use an ultraviolet light source (having a wavelength between 250 and 400 nm), with polymerization that occurs throughout the entirety of the light path. Conversely, 2PP methods utilize near-infrared excitation (between 600 and 1000 nm) to produce high-resolution 3D structures. Here, electronic transitions occur through the simultaneous absorption of two photons, ensuring that radical formation and subsequent polymerization only occur in the immediate vicinity of the focused beam waist, resulting in a small solidified volume (between 30 and 0.4 fL) around the focus. By controlling the location of the voxel in three perpendicular directions (x, y, and z), a three-dimensional structure of any shape can be created in a direct and rapid manner. As long as the incident light intensity is controlled so that the incident light intensity outside the focus is insufficient to produce two-photon absorption, polymerization will be limited to a small region in the vicinity of the optical focus. In this respect, it is important to note that 2PP provides unique advantages over approaches that utilize inertial flow shaping and ultraviolet light polymerization to achieve geometric control.[62] Since many pulsed lasers operate in the near infra-red region of the electromagnetic spectrum, where most curable monomers and polymers are transparent, and because two-photon absorption occurs only in defined spatial regions (where the light intensity is sufficiently high), it is possible to achieve significantly higher light penetration depths. In this way, 2PP will polymerize (and solidify) only a localized portion of the bulk of the liquid resin, without affecting the surrounding region.

Figure 1a illustrates the concept underlying multi-compartment/composition fiber fabrication using 2PP−CFL. Two streams containing the pre-polymer (details provided in Reagents) and methacryloxyethyl thiocarbamoyl rhodamine B-

https://dx.doi.org/10.1021/acsami.0c14917
ACS Appl. Mater. Interfaces 2020, 12, 54068−54074

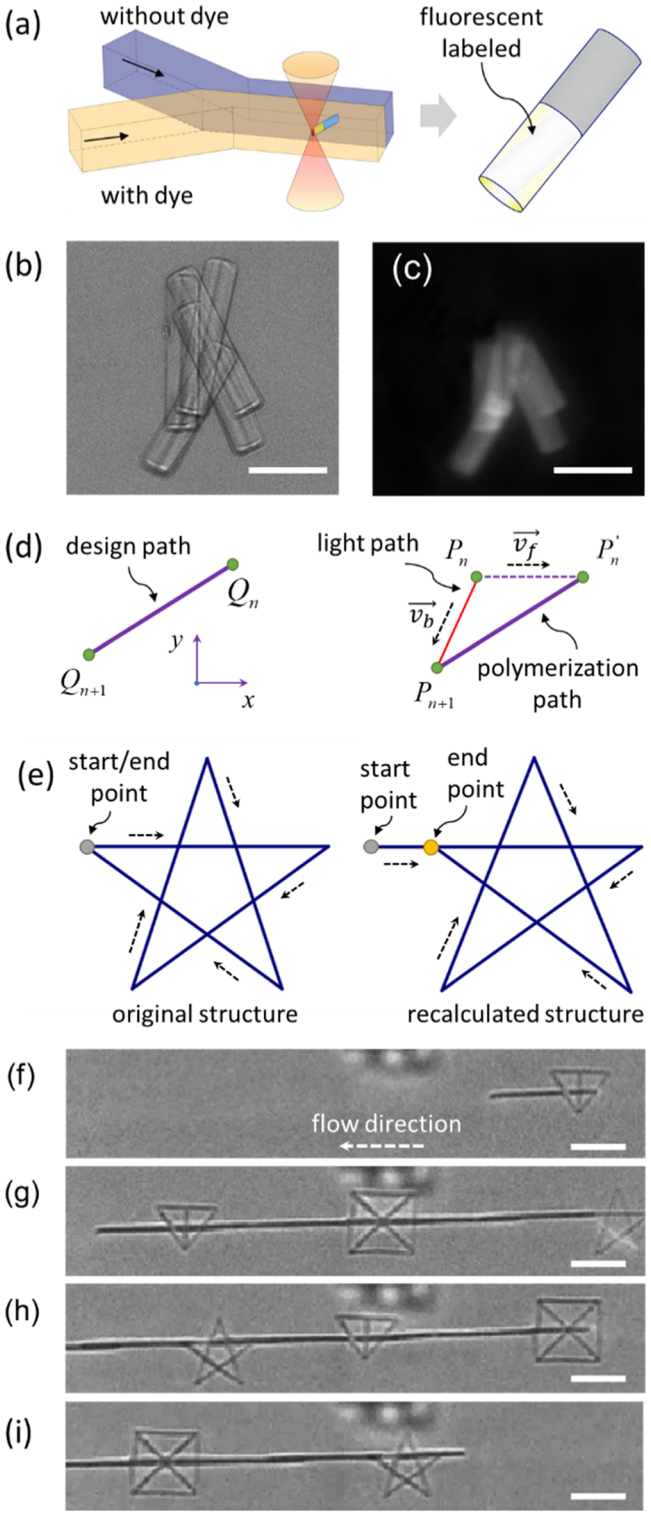

Figure 1. Microfluidic fabrication of functional microfibers. (a) Schematic of the fabrication process. Two types of photoresist are introduced into the primary flow channel, with one photoresist stream containing a fluorophore resonant with the excitation. The laser excitation volume is moved across the interface, solidifying the resist and producing a bespoke, three-dimensional structure. (b) Brightfield image and (c) Fluorescence image of a fiber produced using the described method. Recalculating process for fabricating a single fiber (d) and pentagram frame (e) structures. (f–i) Dynamic brightfield images illustrating the additive manufacturing process occurring under conditional flow conditions. Scale bars are 10 μm in (b,c) and 20 μm in (f–i).

labeled pre-polymer solutions co-flow through within a Y-shaped channel. By controlling the location of the interface (via variations of the volumetric flow rates of the input streams) and the laser-scan path, we are able to robustly synthesize Janus fibers (18 μm long, 5.2 μm high, and 1.6 μm wide) containing spatial color variations at a throughput of 2000 fibers s^{-1}, as shown in the fluorescence and brightfield images in Figure 1b,c. This represents a superior fabrication rate (throughput) than contact flow lithography[63] and with a resolution more than one order of magnitude higher. The schematic presented in Figure 1d indicates the direction of the light path (red line), the polymerized fiber (blue line), and the flow direction (x-direction) under normal operating conditions. Since fabrication occurs under laminar flow conditions, the polymerized material moves at a uniform velocity in the direction of the flow stream. Accordingly, the laser writing path is recalculated as shown in the left panel of Figure 1d. To simplify the writing process, the microfluidic channel is oriented along the x axis allowing the polymerization path to be solved by the following set of equations

$$\begin{cases} P_{n+1} - P_n' = Q_{n+1} - Q_n \\ P_{n+1} - P_n = \vec{v}_b t \\ P_n' - P_n = \vec{v}_f t \end{cases} \quad (1)$$

Here, Q_{n+1} is the coordinate of the end point and Q_n is the starting point of design path, with $\vec{v}_b$ and $\vec{v}_f$ representing the velocity vectors of the beam and flow, respectively. P_{n+1} represents the end point coordinate of the beam path, and P_n and P_n' represent the starting point coordinates of the beam and polymerization paths, respectively. Due to the existence of a finite flow velocity, the original path is divided into two directions $\vec{v}_b$ and $\vec{v}_f$. The free-standing fiber structure is then obtained by scanning the photopolymerization spot, $\vec{v}_b$, and the flow motion, $\vec{v}_f$, of the fluid along the length of the channel (Figure 1d). When the laser-scan path $P_n \rightarrow P_{n+1}$ is used in the flowing medium, the polymerized fiber shifts downstream (from the beam bath) during its construction, ending up in the "real" geometric shape $P_n'P_{n+1}$. Figure 1e presents the recalculating process for a two-dimensional path in the case of a pentagram polymerized structure. By simply flowing two concurrent, laminar streams through the microfluidic device and adopting this polymerization process (incorporating the recalculating method), fibers decorated with different structural patterns can be easily and controllably synthesized (Figure 1f–i).

We applied our 2PP approach for the fabrication of various particle shapes, which can be divided into two categories: solid blocks and frameworks. Figure 2a–i shows the printing paths and the corresponding fluorescence and brightfield images in the case of rectangular (a–c), triangular (d–f), and pentagram solid blocks (g–i, Movie S1), as well as complex pentagram (j–l, Movie S2), rectangular cross (m–o), and triangular frameworks (p–r). The solid and hollow framework objects were fabricated at the rate of 150 and 950 particles s^{-1} respectively. The fabricated cross structures inside the rectangular and the triangular frameworks act to enhance the mechanical strength of the final structures.[64] 3D confocal and brightfield images (Figure S3a,b) of a pentagram framework element demonstrate that the minimum structural element in the generated polymeric objects is approximately 1.5 μm, which represents a one order of magnitude improvement in resolution when compared to SFL.[61] In addition, our fabrication throughput is an order of magnitude

https://dx.doi.org/10.1021/acsami.0c14917
ACS Appl. Mater. Interfaces 2020, 12, 54068–54074

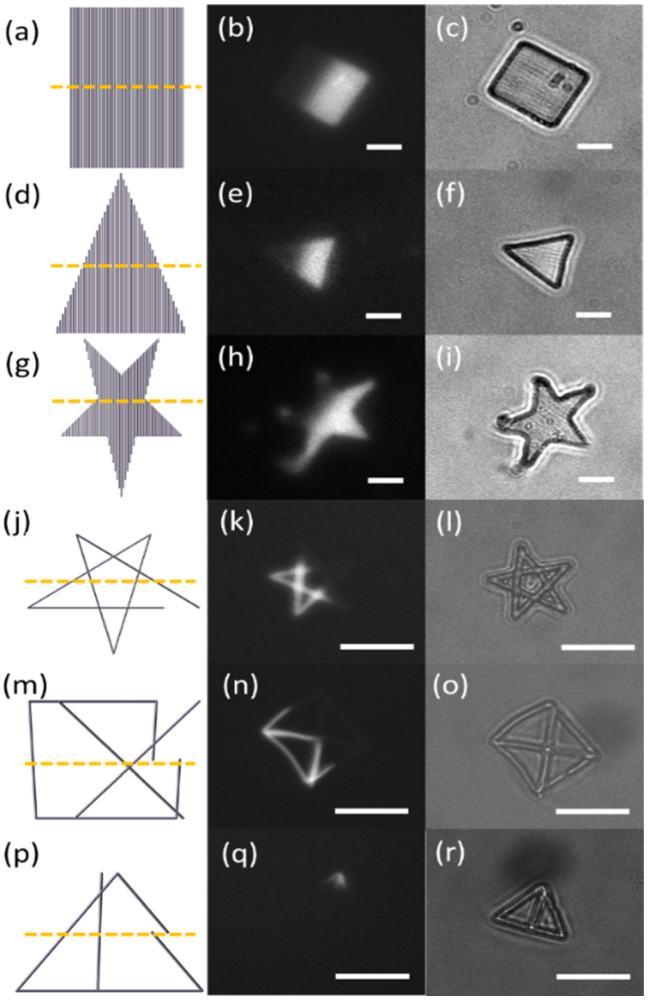

Figure 2. Microstructures formed using two-photon lithography flow lithography. (a–c), (d–f), and (g–i) Printing path, fluorescence image, and the corresponding brightfield image for rectangular, triangular, and star-shaped solid blocks, respectively. (j–l), (m–o), and (p–r) Printing path, fluorescence image, and corresponding brightfield image for pentagram, rectangular, and triangular frameworks, respectively. The dashed lines indicate the laminar flow interfaces. The scale bars are 20 μm.

higher than the fabrication rate of current SFL approaches for similar particle complexities and sizes (14 particles s^{-1}).[61] In this regard, it should be noted that SFL approaches are limited in throughput due to the need to stop the flow of liquid monomer solution in the channel prior to each curing step. Indeed, when fabricating particles with simple or complex structural patterns, our spatial resolution is two orders of magnitude higher than photomask flow lithography based on inertial flow engineering.[65] Moreover, when compared to the throughput of current two-dimensional, two-photon CFL (30 particles s^{-1}),[66] our fabrication rates are at least five times higher, when synthesizing objects of similar geometrical complexity and size.

A recent study by Yuan and co-workers reported that the combination of a thermally drawn transparent fiber template and masked UV-photopolymerization-enabled biaxial control of the fabrication of microstructures with complex geometric features.[61] Although powerful, such an approach lacks flexibility when fabricating extended and structurally complex microfibers. Using the current method, it is possible to polymerize objects at different points along the length of a long fiber within a fluid volume (see Figure 3a). By tuning the volumetric flow rate and laser beam scanning parameters (i.e., scan rate and path), fiber

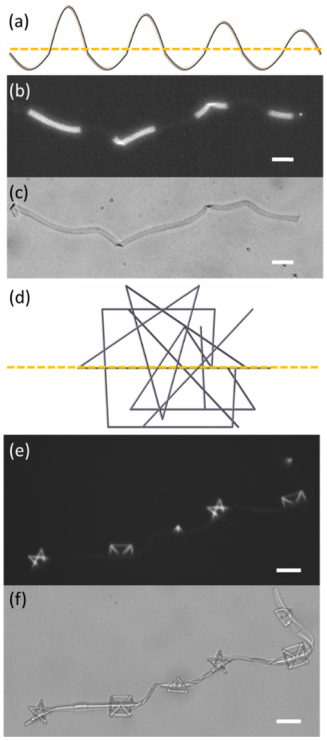

Figure 3. Fabrication of multicomponent materials. (a) Description of the recalculating path for a segmented fiber. (b) Fluorescence image of a functional fiber. (c) Corresponding brightfield image of (b). (d) Design path for a multistructured fiber. (e,f) Fluorescence and brightfield images of multicomponent functional fibers fabricated using the process shown in Figure 1. The dashed lines in (a,d) indicate the laminar flow interfaces. All scale bars in figures are 20 μm.

dimensions can be dynamically tuned during the fabrication process. Indeed, since the length of the resulting fiber is directly proportional to the time that the laser probe beam spends in the corresponding photoresist volume, the length of each segment can be tuned by simply moving the polymerization spot across the interface of different co-flowing solutions in the vertical coordinate. To this end, Figure 3a presents the recalculating path of a length-changing fluorescent functional fiber. Using 2PP–CFL, we were able to construct complex microfibers, approximately 500 μm long and at a rate of 30 fibers s^{-1} (Movie S3). In addition, fabrication of hybrid microfibers with spatial variations in color and structural shapes (rectangles, triangles, and pentagrams) was possible at a rate of 10 fibers s^{-1} (Movie S4), thus expanding their potential as high-performance encoding materials (Figure 3d–f). In addition, it should be noted that the fabrication of hybrid fibers with features as small as 1.5 μm (Figure S3c,d) represents a two order of magnitude improvement in resolution compared to previous fiber synthesis studies[67] and the best reported in the literature to date.

The use of dyes for optical encoding is ultimately compromised by photobleaching. This issue can be mitigated through the introduction of structural codes (in our case, rectangles, triangles, and pentagrams) within individual fibers. As noted, a variety of barcoded particles or fibers incorporating dyes have been reported, and thus, we focused our studies on the creation of hybrid structures that carry both structural and

https://dx.doi.org/10.1021/acsami.0c14917
ACS Appl. Mater. Interfaces 2020, 12, 54068–54074

optical codes and thus mitigate potential issues related to photobleaching.

3. CONCLUSIONS

We have demonstrated a novel method for the fabrication of complex microstructures and fibers consisting of multiple materials and with feature sizes as small as 1.5 μm. In contrast to traditional lithographic techniques, templates can be structured with biaxial control of microparticle and microfiber geometries. To overcome potential "shape shifting" effects caused by flow-based operation, the printing paths are recalculated during the fabricating process. Due to the programmability of the 2PP process, the flexibility and throughput of the fabrication process is greatly enhanced compared to all existing approaches. These capabilities significantly expand the available range of accessible microparticles and microfibers. Indeed, and as previously noted, the purpose of the current study has been to increase the complexity of object geometries and significantly increase fabrication throughput to engender the production of large numbers of arbitrary shapes with submicron-sized feature in a continuous manner. It is important to note that the current polymerization process operates optimally in an X−Y laser scanning mode to fabricate two-dimensional features at high throughput (Figure S4). Notably, multicomponent fibers, through optical and spatial multiplexing, exhibit significant utility in a range of security identification and anticounterfeiting applications.[68−70] A key feature of our method is the ability to fabricate hybrid fibers that encode information via variations in shape, size, and color. Conventional barcoding systems are prone to damage, alteration, or falsification, which may cause a range of security issues for the end user.[71−73] Accordingly, the generation of micron-sized barcodes made from polymers is highly desirable. Such structures can be encoded with bespoke properties with respect to size, shape, and color. Herein, the encoded fibers are made from a hard and inert material via the combination of trimethylolpropane triacrylate (TMPTA) and pentaerythritol triacrylate (PETA) acrylate monomers. Moreover, the ability to encode information on a micron-scale renders them attractive for portable data file applications and real-time labeling and item tracking. In this respect, we believe that 2PP−CFL paves the way for a new generation of functional microscale objects that will enable innovations across a wide variety of application fields.

4. EXPERIMENTAL SECTION

4.1. Reagents. The pre-polymer solution used in all experiments consists of 87% (w/w) trimethylolpropane ethoxylate triacrylate (M_n = 912), 10% (w/w) PETA, and 3% (w/w) IRGACURE 369. To produce fluorescently-labeled fibers, 0.01% of (w/w) methacryloxyethyl thiocarbamoyl rhodamine B (Polyscience Inc., Warrington, USA) was added to the pre-polymer solution. Addition of PETA during synthesis is used to improve the mechanical strength of the fabricated constructs.

4.2. Device Fabrication. The master mold for the Y-shaped microfluidic device was fabricated, using a GT Nanoscribe 3D printer (Nanoscribe GmbH, Eggenstein-Leopoldshafen, Germany) equipped with a 25×, NA 0.8 plan apochromat air objective lens (Zeiss, Oberkochen, Germany), on an ITO-coated glass substrate. The printer is constructed around a two-photon microscope platform. A galvo-resonant scanner controls the laser's x−y focal point within the build space. The cross section of the channel for direct laser writing was 500 μm × 200 μm (width × height). After printing, the mold was developed in propylene glycol methyl ether acetate (Sigma-Aldrich, Buchs, Switzerland) for 20 min, washed in isopropanol for 5 min, and baked in an oven at 200 °C for 2 h. Subsequently, the mold structure was transferred to an elastomeric substrate by pouring SYLGARD 184 polydimethylsiloxane pre-polymer (Dow Corning, Midland, USA) at a 10:1 (w/w) base to curing-agent ratio over the mold and baking at 70 °C for 2 h. Elastomeric replicas were bonded to glass coverslips (160 μm thick) after exposure to an oxygen plasma.

4.3. Device Operation. Two steams of pre-polymer (one containing dye and one without dye) were introduced into a Y-shaped device via two separate inlets at a flow rate of 1 μL min^{-1}, using two precision syringe pumps (neMESYS Syringe Pumps, CETONI GmbH, Korbußen, Germany) (Figure S1). A 25× objective lens was used for both printing and imaging microstructures. In all experiments, the channel bottom is initially identified, and the excitation focus then moved to 100 μm above this level. The galvo-resonant scanner enables the x−y position of excitation beam focus to be controlled in a precise and rapid manner, allowing efficient polymerization of the pre-polymer. The laser power and scanning speed are set as 60 mW and 10 mm s^{-1}, respectively (Figure S2). Polymerized constructs were imaged in both fluorescence and brightfield modes using a Nikon Ti-E microscope (Nikon AG, Egg Switzerland) equipped with an Andor Zyla sCMOS camera (Oxford Instruments, Oxford, UK), with ImageJ (1.47v, National Institutes of Health, USA) being used for image processing. 3D confocal images of the produced structures were obtained using a Nikon C2si microscope confocal microscope (Nikon AG, Egg Switzerland) equipped with a 560 nm laser (Coherent Genesis, Coherent Laser Systems GmbH & Co. KG, Göttingen, Germany). Two objectives at 40× 0.75 NA and 40× 1.2 NA (Nikon AG, Egg Switzerland) were used with a pinhole diameter of 1.05 airy disks. The z plane was scanned with 1 μm step at the top and bottom to span the whole microfiber height. A Rhodamine filter emission (590/50 nm, AHF, Tübingen, Germany) was used as the fluorescence filter.

■ ASSOCIATED CONTENT

Supporting Information

The Supporting Information is available free of charge at https://pubs.acs.org/doi/10.1021/acsami.0c14917.

3D design of the microfluidic chip, laser power parameter screening for determining the resolution of the printed structures, and code for fabricating microstructures using two-photon lithography (PDF)

Printing process of the pentagram solid blocks (MP4)

Printing process of the complex pentagrams (MP4)

Printing process of the segmented fibers (MP4)

Printing process of the hybrid microfiber (MP4)

■ AUTHOR INFORMATION

Corresponding Authors

Stavros Stavrakis − *Institute for Chemical and Bioengineering, ETH Zürich, 8093 Zürich, Switzerland;* orcid.org/0000-0002-0888-5953; Email: stavros.stavrakis@chem.ethz.ch

Andrew J. deMello − *Institute for Chemical and Bioengineering, ETH Zürich, 8093 Zürich, Switzerland;* Email: andrew.demello@chem.ethz.ch

Authors

Xiaobao Cao − *Institute for Chemical and Bioengineering, ETH Zürich, 8093 Zürich, Switzerland;* orcid.org/0000-0003-2211-2823

Quan Gao − *Institute for Chemical and Bioengineering, ETH Zürich, 8093 Zürich, Switzerland; School of Mechanical Engineering, Northwestern Polytechnical University, 710072 Xian, China*

Shangkun Li − *Institute for Chemical and Bioengineering, ETH Zürich, 8093 Zürich, Switzerland*

Songtao Hu − *Institute for Chemical and Bioengineering, ETH Zürich, 8093 Zürich, Switzerland; State Key Laboratory of*

https://dx.doi.org/10.1021/acsami.0c14917
ACS Appl. Mater. Interfaces 2020, 12, 54068−54074

Mechanical System and Vibration, Shanghai Jiao Tong University, 200240 Shanghai, China; orcid.org/0000-0002-8405-3788

Jing Wang − *Institute of Environmental Engineering, ETH Zürich, 8093 Zurich, Switzerland;* orcid.org/0000-0003-2078-137X

Peter Fischer − *Institute of Food Nutrition and Health, ETH Zürich, 8092 Zurich, Switzerland;* orcid.org/0000-0002-2992-5037

Complete contact information is available at: https://pubs.acs.org/10.1021/acsami.0c14917

Author Contributions

The manuscript was written through contributions of all authors. All authors have given approval to the final version of the manuscript. X.C. and Q.G. contributed equally to this work.

Notes

The authors declare no competing financial interest.

■ ACKNOWLEDGMENTS

The authors would like to acknowledge partial financial support from ETH Zürich. X.C. would like to acknowledge the provision of a CSC scholarship. The authors also would like to acknowledge Prerit Mathur and Minghan Hu for their valuable contribution on the acquisition of confocal images.

■ REFERENCES

(1) Braeckmans, K.; De Smedt, S. C.; Leblans, M.; Pauwels, R.; Demeester, J. Encoding Microcarriers: Present and Future Technologies. *Nat. Rev. Drug Discovery* **2002**, *1*, 447−456.

(2) Birtwell, S.; Morgan, H. Microparticle Encoding Technologies for High-Throughput Multiplexed Suspension Assays. *Integr. Biol.* **2009**, *1*, 345−362.

(3) Cederquist, K. B.; Dean, S. L.; Keating, C. D. Encoded Anisotropic Particles for Multiplexed Bioanalysis. *Wiley Interdiscip. Rev.: Nanomed. Nanobiotechnol.* **2010**, *2*, 578−600.

(4) Xiao, X.-Y.; Li, R.; Zhuang, H.; Ewing, B.; Karunaratne, K.; Lillig, J.; Brown, R.; Nicolaou, K. C. Solid-Phase Combinatorial Synthesis Using Microkan Reactors, Rf Tagging, and Directed Sorting. *Biotechnol. Bioeng.* **2000**, *71*, 44−50.

(5) Nicolaou, K. C.; Xiao, X.-Y.; Parandoosh, Z.; Senyei, A.; Nova, M. P. Radiofrequency Encoded Combinatorial Chemistry. *Angew. Chem., Int. Ed.* **1995**, *34*, 2289−2291.

(6) Vaino, A. R.; Janda, K. D. Euclidean Shape-Encoded Combinatorial Chemical Libraries. *Proc. Natl. Acad. Sci. U.S.A.* **2000**, *97*, 7692−7696.

(7) Nicewarner-Pena, S. R.; Freeman, R. G.; Reiss, B. D.; He, L.; Peña, D. J.; Walton, I. D.; Cromer, R.; Keating, C. D.; Natan, M. J. Submicrometer Metallic Barcodes. *Science* **2001**, *294*, 137−141.

(8) Dejneka, M. J.; Streltsov, A.; Pal, S.; Frutos, A. G.; Powell, C. L.; Yost, K.; Yuen, P. K.; Muller, U.; Lahiri, J. Rare Earth-Doped Glass Microbarcodes. *Proc. Natl. Acad. Sci. U.S.A.* **2003**, *100*, 389−393.

(9) Li, Y.; Cu, Y. T. H.; Luo, D. Multiplexed Detection of Pathogen DNA with DNA-Based Fluorescence Nanobarcodes. *Nat. Biotechnol.* **2005**, *23*, 885−889.

(10) Nolan, J. P.; Sklar, L. A. Suspension Array Technology: Evolution of the Flat-Array Paradigm. *Trends Biotechnol.* **2002**, *20*, 9−12.

(11) Fayazpour, F.; Lucas, B.; Huyghebaert, N.; Braeckmans, K.; Derveaux, S.; Stubbe, B. G.; Remon, J.-P.; Demeester, J.; Vervaet, C.; De Smedt, S. C. Digitally Encoded Drug Tablets to Combat Counterfeiting. *Adv. Mater.* **2007**, *19*, 3854−3858.

(12) Lee, H.; Kim, J.; Kim, H.; Kim, J.; Kwon, S. Colour-Barcoded Magnetic Microparticles for Multiplexed Bioassays. *Nat. Mater.* **2010**, *9*, 745−749.

(13) Zhao, Y.; Zhao, X.; Hu, J.; Xu, M.; Zhao, W.; Sun, L.; Zhu, C.; Xu, H.; Gu, Z. Encoded Porous Beads for Label-Free Multiplex Detection of Tumor Markers. *Adv. Mater.* **2009**, *21*, 569−572.

(14) Shikha, S.; Salafi, T.; Cheng, J.; Zhang, Y. Versatile Design and Synthesis of Nano-Barcodes. *Chem. Soc. Rev.* **2017**, *46*, 7054−7093.

(15) Zhao, Y.; Shang, L.; Cheng, Y.; Gu, Z. Spherical Colloidal Photonic Crystals. *Acc. Chem. Res.* **2014**, *47*, 3632−3642.

(16) Leng, Y.; Sun, K.; Chen, X.; Li, W. Suspension Arrays Based on Nanoparticle-Encoded Microspheres for High-Throughput Multiplexed Detection. *Chem. Soc. Rev.* **2015**, *44*, 5552−5595.

(17) Fu, F.; Shang, L.; Zheng, F.; Chen, Z.; Wang, H.; Wang, J.; Gu, Z.; Zhao, Y. Cells Cultured on Core−Shell Photonic Crystal Barcodes for Drug Screening. *ACS Appl. Mater. Interfaces* **2016**, *8*, 13840−13848.

(18) Wilson, R.; Cossins, A. R.; Spiller, D. G. Encoded Microcarriers for High-Throughput Multiplexed Detection. *Angew. Chem., Int. Ed.* **2006**, *45*, 6104−6117.

(19) Pregibon, D. C.; Toner, M.; Doyle, P. S. Multifunctional Encoded Particles for High-Throughput Biomolecule Analysis. *Science* **2007**, *315*, 1393−1396.

(20) Krutzik, P. O.; Nolan, G. P. Fluorescent Cell Barcoding in Flow Cytometry Allows High-Throughput Drug Screening and Signaling Profiling. *Nat. Methods* **2006**, *3*, 361−368.

(21) Li, Y.; Cu, Y. T. H.; Luo, D. Multiplexed Detection of Pathogen DNA with DNA-Based Fluorescence Nanobarcodes. *Nat. Biotechnol.* **2005**, *23*, 885−889.

(22) Lu, J.; Getz, G.; Miska, E. A.; Alvarez-Saavedra, E.; Lamb, J.; Peck, D.; Sweet-Cordero, A.; Ebert, B. L.; Mak, R. H.; Ferrando, A. A.; Downing, J. R.; Jacks, T.; Horvitz, H. R.; Golub, T. R. Microrna Expression Profiles Classify Human Cancers. *Nature* **2005**, *435*, 834−838.

(23) Niehörster, T.; Löschberger, A.; Gregor, I.; Krämer, B.; Rahn, H.-J.; Patting, M.; Koberling, F.; Enderlein, J.; Sauer, M. Multi-Target Spectrally Resolved Fluorescence Lifetime Imaging Microscopy. *Nat. Methods* **2016**, *13*, 257−262.

(24) Valm, A. M.; Cohen, S.; Legant, W. R.; Melunis, J.; Hershberg, U.; Wait, E.; Cohen, A. R.; Davidson, M. W.; Betzig, E.; Lippincott-Schwartz, J. Applying Systems-Level Spectral Imaging and Analysis to Reveal the Organelle Interactome. *Nature* **2017**, *546*, 162−167.

(25) Gorris, H. H.; Ali, R.; Saleh, S. M.; Wolfbeis, O. S. Tuning the Dual Emission of Photon-Upconverting Nanoparticles for Ratiometric Multiplexed Encoding. *Adv. Mater.* **2011**, *23*, 1652−1655.

(26) Zhang, F.; Haushalter, R. C.; Haushalter, R. W.; Shi, Y.; Zhang, Y.; Ding, K.; Zhao, D.; Stucky, G. D. Rare-Earth Upconverting Nanobarcodes for Multiplexed Biological Detection. *Small* **2011**, *7*, 1972−1976.

(27) Fournier-Bidoz, S.; Jennings, T. L.; Klostranec, J. M.; Fung, W.; Rhee, A.; Li, D.; Chan, W. C. Facile and Rapid One-Step Mass Preparation of Quantum-Dot Barcodes. *Angew. Chem., Int. Ed.* **2008**, *47*, 5577−5581.

(28) Han, M.; Gao, X.; Su, J. Z.; Nie, S. Quantum-Dot-Tagged Microbeads for Multiplexed Optical Coding of Biomolecules. *Nat. Biotechnol.* **2001**, *19*, 631−635.

(29) Ji, X.-H.; Cheng, W.; Guo, F.; Liu, W.; Guo, S.-S.; He, Z.-K.; Zhao, X.-Z. On-Demand Preparation of Quantum Dot-Encoded Microparticles Using a Droplet Microfluidic System. *Lab Chip* **2011**, *11*, 2561−2568.

(30) Kim, J.; Biondi, M. J.; Feld, J. J.; Chan, W. C. W. Clinical Validation of Quantum Dot Barcode Diagnostic Technology. *ACS Nano* **2016**, *10*, 4742−4753.

(31) Leng, Y.; Wu, W.; Li, L.; Lin, K.; Sun, K.; Chen, X.; Li, W. Magnetic/Fuorescent Barcodes Based on Cadmium-Free near-Infrared-Emitting Quantum Dots for Multiplexed Detection. *Adv. Funct. Mater.* **2016**, *26*, 7581−7589.

(32) Lawrie, G. A.; Battersby, B. J.; Trau, M. Synthesis of Optically Complex Core−Shell Colloidal Suspensions: Pathways to Multiplexed Biological Screening. *Adv. Funct. Mater.* **2003**, *13*, 887−896.

(33) Sreenath, K.; Yuan, Z.; Allen, J. R.; Davidson, M. W.; Zhu, L. A Fluorescent Indicator for Imaging Lysosomal Zinc(Ii) with Förster

Resonance Energy Transfer (Fret)-Enhanced Photostability and a Narrow Band of Emission. *Chem.—Eur. J.* **2015**, *21*, 867−874.
(34) Cognet, L.; Tardin, C.; Boyer, D.; Choquet, D.; Tamarat, P.; Lounis, B. Single Metallic Nanoparticle Imaging for Protein Detection in Cells. *Proc. Natl. Acad. Sci. U.S.A.* **2003**, *100*, 11350−11355.
(35) Chatten, A. J.; Barnham, K. W. J.; Buxton, B. F.; Ekins-Daukes, N. J.; Malik, M. A. A New Approach to Modelling Quantum Dot Concentrators. *Sol. Energy Mater. Sol. Cells* **2003**, *75*, 363−371.
(36) Nguyen, H. Q.; Baxter, B. C.; Brower, K.; Diaz-Botia, C. A.; DeRisi, J. L.; Fordyce, P. M.; Thorn, K. S. Programmable Microfluidic Synthesis of over One Thousand Uniquely Identifiable Spectral Codes. *Adv. Opt. Mater.* **2017**, *5*, 1600548.
(37) Zhao, Y.; Shum, H. C.; Chen, H.; Adams, L. L. A.; Gu, Z.; Weitz, D. A. Microfluidic Generation of Multifunctional Quantum Dot Barcode Particles. *J. Am. Chem. Soc.* **2011**, *133*, 8790−8793.
(38) Shah, R. K.; Shum, H. C.; Rowat, A. C.; Lee, D.; Agresti, J. J.; Utada, A. S.; Chu, L.-Y.; Kim, J.-W.; Fernandez-Nieves, A.; Martinez, C. J.; Weitz, D. A. Designer Emulsions Using Microfluidics. *Mater. Today* **2008**, *11*, 18−27.
(39) Dendukuri, D.; Doyle, P. S. The Synthesis and Assembly of Polymeric Microparticles Using Microfluidics. *Adv. Mater.* **2009**, *21*, 4071−4086.
(40) Cheng, Y.; Zheng, F.; Lu, J.; Shang, L.; Xie, Z.; Zhao, Y.; Chen, Y.; Gu, Z. Bioinspired Multicompartmental Microfibers from Microfluidics. *Adv. Mater.* **2014**, *26*, 5184−5190.
(41) Shum, H. C.; Abate, A. R.; Lee, D.; Studart, A. R.; Wang, B.; Chen, C.-H.; Thiele, J.; Shah, R. K.; Krummel, A.; Weitz, D. A. Droplet Microfluidics for Fabrication of Non-Spherical Particles. *Macromol. Rapid Commun.* **2010**, *31*, 108−118.
(42) Zhao, Y.; Cheng, Y.; Shang, L.; Wang, J.; Xie, Z.; Gu, Z. Microfluidic Synthesis of Barcode Particles for Multiplex Assays. *Small* **2015**, *11*, 151−174.
(43) Dendukuri, D.; Gu, S. S.; Pregibon, D. C.; Hatton, T. A.; Doyle, P. S. Stop-Flow Lithography in a Microfluidic Device. *Lab Chip* **2007**, *7*, 818−828.
(44) Dendukuri, D.; Pregibon, D. C.; Collins, J.; Hatton, T. A.; Doyle, P. S. Continuous-Flow Lithography for High-Throughput Microparticle Synthesis. *Nat. Mater.* **2006**, *5*, 365−369.
(45) Chung, S. E.; Park, W.; Park, H.; Yu, K.; Park, N.; Kwon, S. Optofluidic Maskless Lithography System for Real-Time Synthesis of Photopolymerized Microstructures in Microfluidic Channels. *Appl. Phys. Lett.* **2007**, *91*, 041106.
(46) Lee, J.; Bisso, P. W.; Srinivas, R. L.; Kim, J. J.; Swiston, A. J.; Doyle, P. S. Universal Process-Inert Encoding Architecture for Polymer Microparticles. *Nat. Mater.* **2014**, *13*, 524−529.
(47) Chapin, S. C.; Doyle, P. S. Ultrasensitive Multiplexed Microrna Quantification on Encoded Gel Microparticles Using Rolling Circle Amplification. *Anal. Chem.* **2011**, *83*, 7179−7185.
(48) Frenzel, T.; Kadic, M.; Wegener, M. Three-Dimensional Mechanical Metamaterials with a Twist. *Science* **2017**, *358*, 1072−1074.
(49) Laza, S. C.; Polo, M.; Neves, A. A. R.; Cingolani, R.; Camposeo, A.; Pisignano, D. Two-Photon Continuous Flow Lithography. *Adv. Mater.* **2012**, *24*, 1304−1308.
(50) Kang, E.; Jeong, G. S.; Choi, Y. Y.; Lee, K. H.; Khademhosseini, A.; Lee, S.-H. Digitally Tunable Physicochemical Coding of Material Composition and Topography in Continuous Microfibres. *Nat. Mater.* **2011**, *10*, 877−883.
(51) Jun, Y.; Kang, E.; Chae, S.; Lee, S.-H. Microfluidic Spinning of Micro-and Nano-Scale Fibers for Tissue Engineering. *Lab Chip* **2014**, *14*, 2145−2160.
(52) Cheng, J.; Jun, Y.; Qin, J.; Lee, S.-H. Electrospinning Versus Microfluidic Spinning of Functional Fibers for Biomedical Applications. *Biomaterials* **2017**, *114*, 121−143.
(53) Cheng, Y.; Yu, Y.; Fu, F.; Wang, J.; Shang, L.; Gu, Z.; Zhao, Y. Controlled Fabrication of Bioactive Microfibers for Creating Tissue Constructs Using Microfluidic Techniques. *ACS Appl. Mater. Interfaces* **2016**, *8*, 1080−1086.
(54) Nie, M.; Takeuchi, S. Microfluidics Based Synthesis of Coiled Hydrogel Microfibers with Flexible Shape and Dimension Control. *Sens. Actuators, B* **2017**, *246*, 358−362.
(55) Shin, S.-J.; Park, J.-Y.; Lee, J.-Y.; Park, H.; Park, Y.-D.; Lee, K.-B.; Whang, C.-M.; Lee, S.-H. "On the Fly" Continuous Generation of Alginate Fibers Using a Microfluidic Device. *Langmuir* **2007**, *23*, 9104−9108.
(56) Onoe, H.; Okitsu, T.; Itou, A.; Kato-Negishi, M.; Gojo, R.; Kiriya, D.; Sato, K.; Miura, S.; Iwanaga, S.; Kuribayashi-Shigetomi, K.; Matsunaga, Y. T.; Shimoyama, Y.; Takeuchi, S. Metre-Long Cell-Laden Microfibres Exhibit Tissue Morphologies and Functions. *Nat. Mater.* **2013**, *12*, 584−590.
(57) Yu, Y.; Wen, H.; Ma, J.; Lykkemark, S.; Xu, H.; Qin, J. Flexible Fabrication of Biomimetic Bamboo-Like Hybrid Microfibers. *Adv. Mater.* **2014**, *26*, 2494−2499.
(58) Tottori, S.; Takeuchi, S. Formation of Liquid Rope Coils in a Coaxial Microfluidic Device. *RSC Adv.* **2015**, *5*, 33691−33695.
(59) Hwang, C. M.; Khademhosseini, A.; Park, Y.; Sun, K.; Lee, S.-H. Microfluidic Chip-Based Fabrication of Plga Microfiber Scaffolds for Tissue Engineering. *Langmuir* **2008**, *24*, 6845−6851.
(60) Yu, Y.; Wei, W.; Wang, Y.; Xu, C.; Guo, Y.; Qin, J. Simple Spinning of Heterogeneous Hollow Microfibers on Chip. *Adv. Mater.* **2016**, *28*, 6649−6655.
(61) Yuan, R.; Nagarajan, M. B.; Lee, J.; Voldman, J.; Doyle, P. S.; Fink, Y. Designable 3d Microshapes Fabricated at the Intersection of Structured Flow and Optical Fields. *Small* **2018**, *14*, 1803585.
(62) Paulsen, K. S.; Di Carlo, D.; Chung, A. J. Optofluidic Fabrication for 3d-Shaped Particles. *Nat. Commun.* **2015**, *6*, 6976.
(63) Le Goff, G. C.; Lee, J.; Gupta, A.; Hill, W. A.; Doyle, P. S. High-Throughput Contact Flow Lithography. *Adv. Sci.* **2015**, *2*, 1500149.
(64) Klein, F.; Richter, B.; Striebel, T.; Franz, C. M.; Freymann, G. v.; Wegener, M.; Bastmeyer, M. Two-Component Polymer Scaffolds for Controlled Three-Dimensional Cell Culture. *Adv. Mater.* **2011**, *23*, 1341−1345.
(65) Paulsen, K. S.; Di Carlo, D.; Chung, A. J. Optofluidic Fabrication for 3d-Shaped Particles. *Nat. Commun.* **2015**, *6*, 6976.
(66) Shaw, L. A.; Chizari, S.; Shusteff, M.; Naghsh-Nilchi, H.; Di Carlo, D.; Hopkins, J. B. Scanning Two-Photon Continuous Flow Lithography for Synthesis of High-Resolution 3d Microparticles. *Opt. Express* **2018**, *26*, 13543−13548.
(67) Kang, E.; Jeong, G. S.; Choi, Y. Y.; Lee, K. H.; Khademhosseini, A.; Lee, S.-H. Digitally Tunable Physicochemical Coding of Material Composition and Topography in Continuous Microfibres. *Nat. Mater.* **2011**, *10*, 877−883.
(68) Zijlstra, P.; Chon, J. W. M.; Gu, M. Five-Dimensional Optical Recording Mediated by Surface Plasmons in Gold Nanorods. *Nature* **2009**, *459*, 410−413.
(69) Meruga, J. M.; Cross, W. M.; Stanley May, P.; Luu, Q.; Crawford, G. A.; Kellar, J. J. Security Printing of Covert Quick Response Codes Using Upconverting Nanoparticle Inks. *Nanotechnology* **2012**, *23*, 395201.
(70) Lu, Y.; Zhao, J.; Zhang, R.; Liu, Y.; Liu, D.; Goldys, E. M.; Yang, X.; Xi, P.; Sunna, A.; Lu, J.; Shi, Y.; Leif, R. C.; Huo, Y.; Shen, J.; Piper, J. A.; Robinson, J. P.; Jin, D. Tunable Lifetime Multiplexing Using Luminescent Nanocrystals. *Nat. Photonics* **2013**, *8*, 32−36.
(71) Prime, E. L.; Solomon, D. H. Australia's Plastic Banknotes: Fighting Counterfeit Currency. *Angew. Chem., Int. Ed.* **2010**, *49*, 3726−3736.
(72) Aldhous, P. Murder by Medicine. *Nature* **2005**, *434*, 132−134.
(73) Hardwick, B.; Jackson, W.; Wilson, G.; Mau, A. W. H. Advanced Materials for Banknote Applications. *Adv. Mater.* **2001**, *13*, 980−984.

https://dx.doi.org/10.1021/acsami.0c14917
ACS Appl. Mater. Interfaces 2020, 12, 54068−54074